IOPscience iopscience.iop.org

Home Search Collections Journals About Contact us My IOPscience

Effect of Growth Temperature on Formation of Amorphous Nitride Interlayer between AlN and Si(111)

This content has been downloaded from IOPscience. Please scroll down to see the full text.

2013 Jpn. J. Appl. Phys. 52 08JB20

(http://iopscience.iop.org/1347-4065/52/8S/08JB20)

View the table of contents for this issue, or go to the journal homepage for more

Download details:

IP Address: 140.113.38.11
This content was downloaded on 25/04/2014 at 09:09

Please note that terms and conditions apply.

Japanese Journal of Applied Physics **52** (2013) 08JB20 **REGULAR PAPER**
http://dx.doi.org/**10.7567/JJAP.52.08JB20**

Effect of Growth Temperature on Formation of Amorphous Nitride Interlayer between AlN and Si(111)

Pei-Yin Lin*, Jr-Yu Chen, Yu-Chang Chen, and Li Chang*

Department of Materials Science and Engineering, National Chiao Tung University, Hsinchu 30010, Taiwan
E-mail: pylin.mse98g@nctu.edu.tw; lichang@cc.nctu.edu.tw

Received October 13, 2012; revised December 3, 2012; accepted January 28, 2013; published online May 31, 2013

The formation of an amorphous interlayer between AlN and Si(111), which may degrade the film quality, is studied by varying the substrate temperature from 860 to 1010 °C in metal–organic chemical vapor deposition with a preflow of trimethylaluminum. The microstructure and chemistry of the amorphous interlayer have been investigated using transmission electron microscopy (TEM) and X-ray photoelectron spectroscopy (XPS). Cross-sectional TEM examinations show that AlN is directly in contact with Si for growth at 860 °C. At higher growth temperatures, an amorphous interlayer can be formed even if an AlN layer has been previously deposited on Si, and its thickness increases with growth temperature. The XPS depth profile across the amorphous interlayer formed at 1010 °C shows that both Al and N exhibit similar distribution, which gradually decreases toward the Si substrate whereas the Si concentration has the opposite distribution. The composition of the amorphous interlayer is determined to consist of Al, Si, and N. © 2013 The Japan Society of Applied Physics

1. Introduction

Recent developments have shown that GaN on Si can be realized in practical applications for power electronic devices and light-emitting devices with low cost and large area wafer size.[1–5] The direct growth of high-quality GaN(0001) on Si(111) is greatly hindered by the large mismatch in lattice parameters and thermal stress due to the difference in thermal expansion coefficients, which usually result in poor crystallinity of the GaN film. AlN is generally used as a buffer layer for GaN epitaxy on Si substrate to prevent a meltback reaction between Si and Ga, and to reduce the dislocation density.[6–9] An important challenge for the growth of III–nitrides on Si is to eliminate the amorphous interlayer formed at the AlN/Si interface, which may degrade the film quality.[10–13] Previous studies of GaN growth on Si show no interlayer between AlN and Si using a preflow of trimethylaluminum (TMA) in metal–organic chemical vapor deposition (MOCVD).[14] Recently, Radtke et al. have grown AlN on Si(111) by metal–organic vapor phase epitaxy with TMA preflow at 735 and 1040 °C.[15,16] Their results show that an amorphous interlayer can still be formed at the AlN/Si interface even though TMA preflow has been applied to the Si surface for a few seconds. To date, the mechanism for the formation of the amorphous interlayer and its composition is not clear.[15–20] Hence, we design a two-step method of growth at different temperatures and systematically study the temperature influence of MOCVD on the formation of the amorphous interlayer. The microstructure and chemistry of the amorphous interlayer have been investigated using high-resolution transmission electron microscopy (HRTEM) with X-ray energy dispersive spectroscopy (EDS) and X-ray photoelectron spectroscopy (XPS). These experimental results provide a better understanding of the structure of the AlN/Si interface and bring further insight into the important role of growth temperature on the formation of the amorphous interlayer which has been determined to consist of Al, Si, and N.

2. Experimental Methods

All the samples were grown on 2-in. Si(111) substrates miscut 4° toward ⟨110⟩ by MOCVD in an Emcore D-180 reactor. The 2-in. Si(111) substrates were cleaned with dilute HF to remove the contaminants and native oxide. Before AlN deposition, the Si(111) substrate was first annealed in the reactor at 1000 °C under hydrogen ambient to remove any residual oxide. TMA was used as a group-III precursor with a carrier gas of hydrogen, while ammonia was used as the nitrogen source. For the first sample, TMA preflow at 860 °C for 15 s was applied to the Si substrate, followed by the growth of an AlN layer at the same temperature for 60 min. The other two samples were deposited by a two-step method in which the first step was TMA preflow at 860 °C for 15 s, followed by the growth of a nucleation AlN layer at the same temperature for 6 min. After the growth of the nucleation layer, the second step consisted of TMA preflow for 15 s at 920 and 1010 °C, followed by further growth of AlN for 60 min at the same temperature, respectively, for the second and third samples. A V/III ratio of 700 and a reactor pressure of 50 Torr were used for AlN growth. The crystallinities of all the samples were examined with X-ray diffraction (XRD). Cross-sectional transmission electron microscopy (TEM) specimens were prepared in an FEI NOVA-200 focused ion beam system using a 30 kV Ga^+ source. The structural characterization at atomic scale was performed in a JEOL JEM-ARM200F spherical aberration corrected scanning transmission electron microscope. The XPS chemical analysis was performed in a PHI Quantera SXM/AES650 system (Al Kα), and 1 kV Ar ion beam sputtering on a $1 \times 1\ mm^2$ area was used for acquiring a depth profile with the sputtering rate of roughly 4 nm/min.

3. Results and Discussion

XRD shows that the first sample of AlN grown at 860 °C is *c*-plane oriented with a full width at half maximum (FWHM) of the (0002) X-ray rocking curve of 1.5°. TEM observations with the selected area diffraction pattern confirm that the AlN film is epitaxial on Si with an orientation relationship of $\{0001\}_{AlN} \parallel \{111\}_{Si}$ and $\langle 11\bar{2}0\rangle_{AlN} \parallel \langle 110\rangle_{Si}$ and the film thickness is 230 nm corresponding to a growth rate of 3.8 nm/min. Figure 1(a) shows a cross-sectional HRTEM image taken from the interfacial region between the AlN film and the Si substrate from which Si(111) lattice fringes can be seen parallel to AlN(0002) ones and an abrupt

 © 2013 The Japan Society of Applied Physics

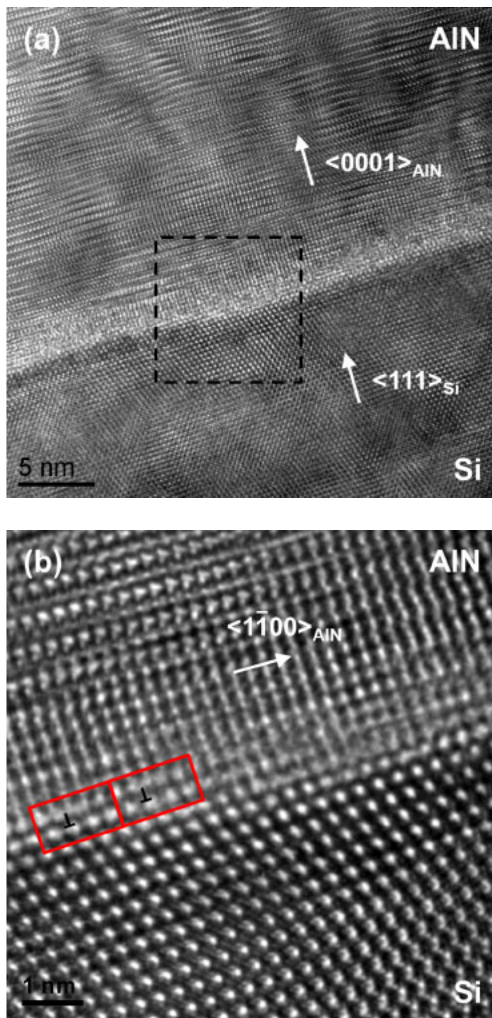

Fig. 1. (Color online) Cross-sectional HRTEM image of AlN epilayer on Si(111) substrate. Growth condition: 15 s TMA preflow and 60 min AlN growth at 860 °C (the first sample). (a) No amorphous interlayer was observed at the interface of AlN and Si. (b) Fourier-filtered image of the framed region in (a). Zone axis $\parallel \langle 11\bar{2}0\rangle_{AlN} \parallel \langle 110\rangle_{Si}$.

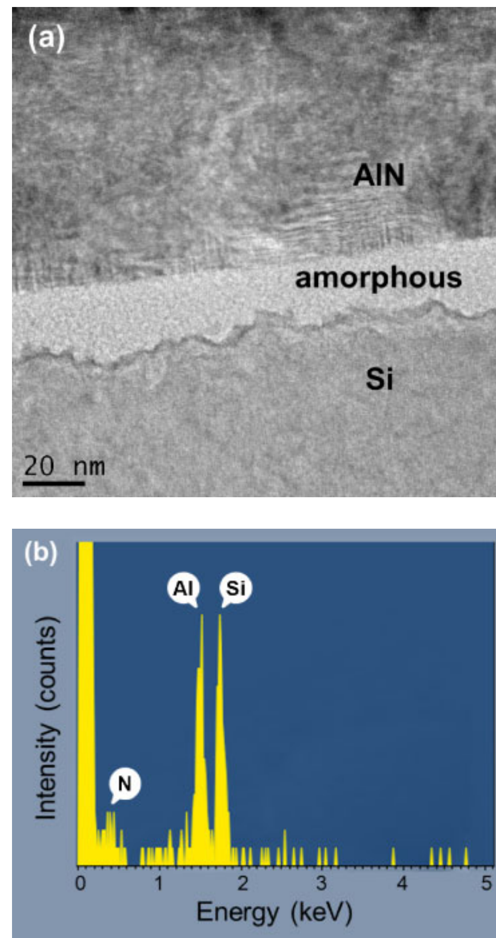

Fig. 2. (Color online) (a) Cross-sectional bright field TEM image of the third sample grown by the two-step method showing a 25-nm-thick amorphous interlayer between AlN and Si. Growth condition: the first step was 15 s TMA preflow and 6 min AlN growth at 860 °C, and the second step was 15 s TMA preflow and 60 min AlN growth at 1010 °C. (b) Nanobeam EDS spectrum of the middle of the amorphous interlayer showing Al, Si, and N peaks.

interface between the AlN layer and the Si substrate is observed without any interlayer. Figure 1(b) shows the Fourier-filtered image of the framed region in Fig. 1(a), revealing that the large lattice mismatch between Si(111) and AlN(0002) can be accommodated by the formation of a regular network of misfit dislocations with an approximate 5 : 4 coincidence between $\{1\bar{1}00\}_{AlN}$ and $\{111\}_{Si}$ planes.[21)]

For the samples grown by the two-step method, XRD and cross-sectional TEM show that all the deposited AlN films are in epitaxy with Si. Also, we have used cross-sectional TEM to show that a 25-nm-thick nucleation AlN layer has been directly deposited on Si without the formation of an amorphous interlayer after the first step growth. When the growth temperature is raised to 920 °C in the second step (the second sample), it can be shown by HRTEM (not shown here) that a 2-nm-thick amorphous interlayer exists between AlN and Si. For a growth temperature of over 1000 °C in the second step (the third sample), an amorphous interlayer of 25 nm thickness is clearly observed between AlN and Si, as shown in Fig. 2(a), in spite of using the TMA preflow. In Fig. 2(b), nanobeam chemical analysis by TEM/EDS on the middle of the amorphous interlayer reveals that Al, Si, and N coexist in this region. It is also observed that the interface between the AlN thin film and the amorphous AlSiN interlayer is sharp and flat, implying that it is fairly stable. In contrast, the interface between the amorphous AlSiN interlayer and Si is very rough, probably owing to its instability resulting from Si outdiffusion and reaction with Al and N. From the above results, it is clear that the formation of the amorphous interlayer occurs in the second step, which raises the growth temperature above 860 °C, and the amorphous interlayer thickness increases with the AlN growth temperature on which diffusion and reaction rates are dependent. The FWHM of the (0002) X-ray rocking curve of the third sample increases to 1.8°, indicating that the formation of an amorphous interlayer results in the degradation of AlN film crystallinity.

The XPS depth profile of the third sample across the amorphous interlayer is shown in Fig. 3, illustrating that both Al and N exhibit similar distribution, which gradually decreases toward the Si substrate whereas the Si concentration has the opposite distribution. It is suggested that the interdiffusion of Si, Al, and N may occur during interlayer formation, even if a 25 nm AlN nucleation layer has already

© 2013 The Japan Society of Applied Physics

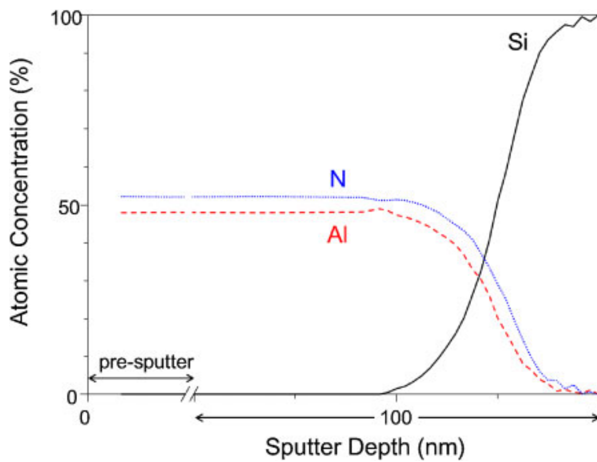

Fig. 3. (Color online) XPS depth profile across the amorphous interlayer formed at 1010 °C in the third sample showing distribution of Si, Al, and N concentrations. Note that the original point of sputtering time is not from the surface of the AlN layer, which has been pre-sputtered for tens of nanometer thickness.

been formed on Si in the first step at 860 °C. The reason for this could be that the AlN layer with lower crystallinity is not an effective diffusion barrier to Si, Al, and N. The XPS Si 2p, Al 2p, and N 1s signals from AlN, the amorphous interlayer, and Si in the third sample are shown Fig. 4. There is no apparent difference in the peak binding energy of Si 2p between Si and the amorphous interlayer, implying that most of the Si atoms in the AlSiN layer have similar bonding characteristics to those in bulk Si. However, asymmetrical distribution of the Si 2p curve can be recognized for the AlSiN, and the curve fitting reveals that there exists an additional peak at >100 eV, which is close to the Si 2p binding energy in Si_3N_4. Comparison of the Al 2p and N 1s binding energies of AlN with the amorphous AlSiN interlayer shows that there is a chemical shift from 73.4 to 74.0 eV for Al 2p and from 396.6 to 397.2 eV for N 1s, suggesting that the interlayer composition is different from AlN and Si_3N_4 because Al 2p and N 1s for AlN are less than 73.7 and 396.8 eV, respectively, and N 1s for SiN_x ~397.8 eV.[22] The N bonding in the AlSiN film may be close to that in SiN_x, and the difference between Si 2p and N 1s is ~295.8 eV in AlSiN similar to that in SiN_x. Similar chemical shifts for Al, Si, and N have been reported in the XPS studies of sputtered AlSiN films by Pélisson-Schecker et al.[22,23] and Maeno et al.[24] From the above results of EDS and XPS depth profile, it is evident that the interlayer is actually composed of Al, Si, and N.

Previous studies have shown that TMA preflow on Si can prevent amorphous silicon nitride formation. Our results clearly demonstrate that the AlN film grown directly on Si can be achieved at relatively low temperature. However, the existence of an AlN nucleation layer with TMA preflow cannot guarantee further growth of AlN without amorphous AlSiN formation at high temperature. As the AlSiN layer thickness increases with growth temperature and the AlSiN has different bonding characteristics and composition from AlN and silicon nitride, it is evident that the AlSiN itself is not as silicon nitride as an effective diffusion barrier to silicon, nitrogen and hydrogen because the growth of silicon

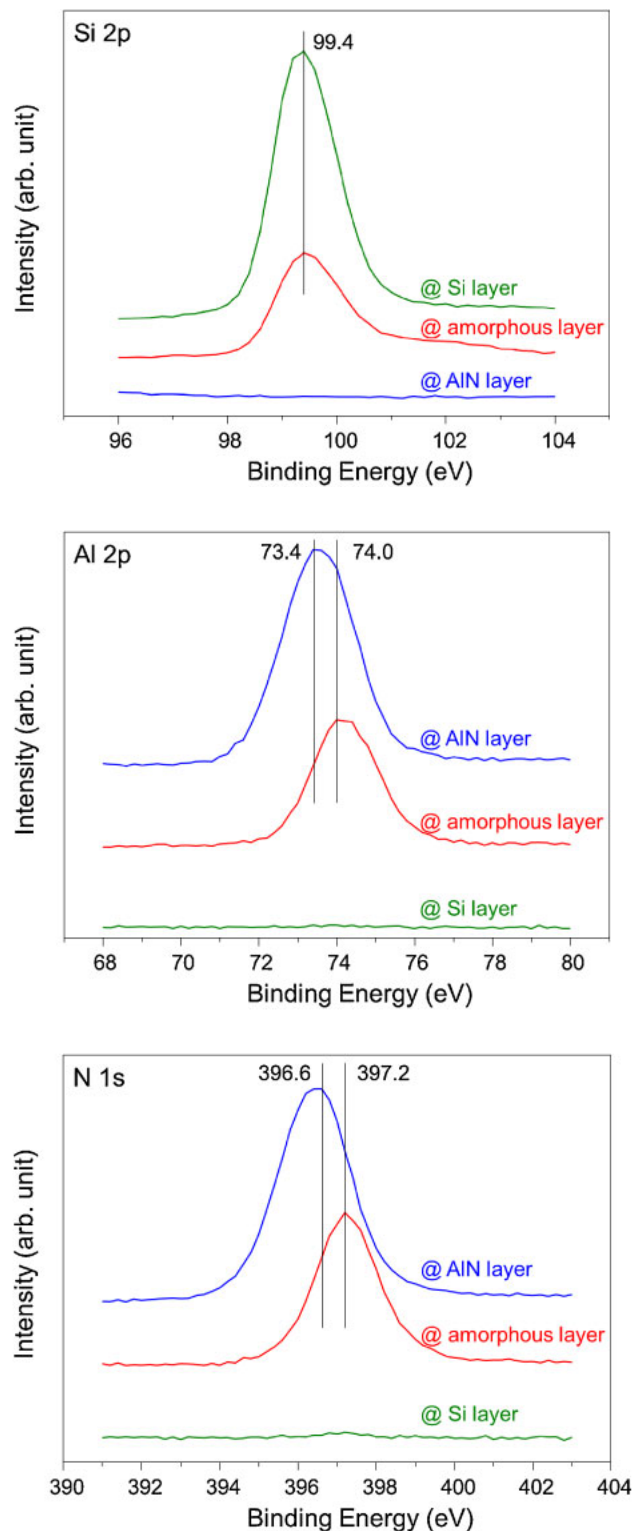

Fig. 4. (Color online) Comparison of binding energies of Si 2p, Al 2p, and N 1s in AlN, amorphous interlayer, and Si in the third sample.

nitride is self-limited in the nitridation process of Si by NH_3.[25,26] As a result, interdiffusion and reaction among Al, Si, and N during MOCVD growth of AlN may occur to form amorphous AlSiN between AlN and Si. Since both diffusion and reaction rates increase with growth temperature, the increase of AlSiN layer thickness with temperature is reasonable. In general, better crystallinity of AlN requires growth at a high temperature, which may result in the

© 2013 The Japan Society of Applied Physics

inevitable formation of an amorphous interlayer. Although we have shown the condition of the formation of an amorphous interlayer with its chemical composition, further investigation for understanding the mechanism of the formation of the amorphous AlSiN interlayer is still required, which will be beneficial for quality improvements of AlN on Si.

4. Conclusions

In this work, the direct growth of a 230-nm-thick AlN epilayer on Si(111) at 860 °C with TMA preflow has been demonstrated without the formation of any amorphous interlayer. For the two-step growth of the AlN layer, the 25 nm AlN nucleation layer grown in the first step at 860 °C cannot prevent further AlN growth from the formation of an amorphous interlayer at the AlN/Si interface in the second step at 920 and 1010 °C. Cross-sectional TEM/EDS and the XPS depth profile across the amorphous interlayer prove that the amorphous interlayer is composed of Al, Si, and N.

Acknowledgements

This work was supported by the National Science Council (NSC 99-2221-E-009-111), the Ministry of Economic Affairs (99-EC-17-A-05-S1-154), and National Chiao Tung University (100W978, 101W978).

1) A. Krost and A. Dadgar: Mater. Sci. Eng. B **93** (2002) 77.
2) S. L. Selvaraj, T. Suzue, and T. Egawa: IEEE Electron Device Lett. **30** (2009) 587.
3) T. Egawa and B. A. B. Ahmad Shuhaimi: J. Phys. D **43** (2010) 354008.
4) S. Fujikawa and H. Hirayama: Appl. Phys. Express **4** (2011) 061002.
5) K. Cheng, H. Liang, M. Van Hove, K. Geens, B. De Jaeger, P. Srivastava, X. Kang, P. Favia, H. Bender, S. Decoutere, J. Dekoster, J. Ignacio del Agua Borniquel, S. W. Jun, and H. Chung: Appl. Phys. Express **5** (2012) 011002.
6) S. Karmann, H. P. D. Schenk, U. Kaiser, A. Fissel, and Wo Richter: Mater. Sci. Eng. B **50** (1997) 228.
7) H. Lahrèche, P. Vennéguès, O. Tottereau, M. Laügt, P. Lorenzini, M. Leroux, B. Beaumont, and P. Gibart: J. Cryst. Growth **217** (2000) 13.
8) A. Dadgar, F. Schulze, M. Wienecke, A. Gadanecz, J. Bläsing, P. Veit, T. Hempel, A. Diez, J. Christen, and A. Krost: New J. Phys. **9** (2007) 389.
9) A. Ubukata, K. Ikenaga, N. Akutsu, A. Yamaguchi, K. Matsumoto, T. Yamazaki, and T. Egawa: J. Cryst. Growth **298** (2007) 198.
10) S. Kaiser, M. Jakob, J. Zweck, W. Gebhardt, O. Ambacher, R. Dimitrov, A. T. Schremer, J. A. Smart, and J. R. Shealy: J. Vac. Sci. Technol. B **18** (2000) 733.
11) M. H. Kim, Y. C. Bang, N. M. Park, C. J. Choi, T. Y. Seong, and S. J. Park: Appl. Phys. Lett. **78** (2001) 2858.
12) K. Cheng, M. Leys, S. Degroote, B. Van Daele, S. Boeykens, J. Derluyn, M. Germain, G. Van Tendeloo, J. Engelen, and G. Borghs: J. Electron. Mater. **35** (2006) 592.
13) J. Borysiuk, P. Caban, W. Strupiński, S. Gierlotka, S. Stelmakh, and J. F. Janik: Cryst. Res. Technol. **42** (2007) 1291.
14) R. Liu, F. A. Ponce, A. Dadgar, and A. Krost: Appl. Phys. Lett. **83** (2003) 860.
15) G. Radtke, M. Couillard, G. A. Botton, D. Zhu, and C. J. Humphreys: Appl. Phys. Lett. **97** (2010) 251901.
16) G. Radtke, M. Couillard, G. A. Botton, D. Zhu, and C. J. Humphreys: Appl. Phys. Lett. **100** (2012) 011910.
17) S. Tanaka, Y. Kawaguchi, N. Sawaki, M. Hibino, and K. Hiramatsu: Appl. Phys. Lett. **76** (2000) 2701.
18) A. Le Louarn, S. Vézian, F. Semond, and J. Massies: J. Cryst. Growth **311** (2009) 3278.
19) E. Arslan, M. K. Ozturk, Ö. Duygulu, A. Arslan Kaya, S. Ozcelik, and E. Ozbay: Appl. Phys. A **94** (2009) 73.
20) E. Arslan, Ö. Duygulu, A. Arslan Kaya, A. Teke, S. Özçelik, and E. Ozbay: Superlattices Microstruct. **46** (2009) 846.
21) K. Y. Zang, L. S. Wang, S. J. Chua, and C. V. Thompson: J. Cryst. Growth **268** (2004) 515.
22) A. Pélisson-Schecker, H. J. Hug, and J. Patscheider: Surf. Interface Anal. **44** (2012) 29.
23) A. Pélisson-Schecker, H. J. Hug, and J. Patscheider: J. Appl. Phys. **108** (2010) 023508.
24) Y. Maeno, M. Kobayashi, K. Oishi, and K. Kawamura: IEEE Trans. J. Magn. Jpn. **5** (1990) 59.
25) I. J. R. Baumvol, F. C. Stedile, J.-J. Ganem, S. Rigo, and I. Trimaille: J. Electrochem. Soc. **142** (1995) 1205.
26) R. M. C. de Almeida and I. J. R. Baumvol: Phys. Rev. B **62** (2000) R16255.

© 2013 The Japan Society of Applied Physics